JOURNAL OF SOLID STATE CHEMISTRY 119, 62–67 (1995)

Vapor Pressure Scanning of Oxygen Nonstoichiometry in $YBa_2Cu_3O_y$

V. N. Guskov, I. V. Tarasov, and V. B. Lazarev

Kurnakov Institute of General and Inorganic Chemistry, Russian Academy of Sciences, Moscow, Russia

and

J. H. Greenberg[1]

Department of Inorganic and Analytical Chemistry, Hebrew University, 91904 Jerusalem, Israel

Received November 28, 1994; accepted March 23, 1995

Oxygen nonstoichiometry in high-T_c superconductor $YBa_2Cu_3O_y$ was studied by vapor pressure measurements in a closed volume in the temperature range 673 to 1173 K and oxygen pressure up to 1 atm. *P–T–X* phase relationships were derived from the vapor pressure scanning of the solidus surface. Analytical representation of isothermal, isobaric, and isoplethal (X_s = const) sections of the *P–T–X* diagram is given. Partial thermodynamic functions of oxygen were calculated in the oxygen nonstoichiometry range 6.30 to 6.85. © 1995 Academic Press, Inc.

1. INTRODUCTION

$YBa_2Cu_3O_y$ has been studied in more detail as compared to other high-temperature superconductor oxides. The region of oxygen nonstoichiometry in this phase was shown to be rather wide (y = 6.0 to 7.0). It was proved to be the main factor determining the superconducting properties of this compound. Thus, dependence of the oxygen index on temperature and vapor pressure, or the *P–T–X* region of existence of the $YBa_2Cu_3O_y$ phase, is crucial for the technology of this material.

Several thermogravimetric studies of oxygen nonstoichiometry in $YBa_2Cu_3O_y$ have been published (1–5). In the present paper we report the results of the direct oxygen vapor pressure measurement in a closed volume at temperatures 673 to 1173 K and oxygen pressures 1 to 760 mm Hg, which span the oxygen nonstoichiometry range 6.2 to 6.97.

2. EXPERIMENTAL

2.1. Sample Preparation

The samples were prepared via solid-state reaction procedure from Y_2O_3 (analytical grade, calcined at 1173 K in air), $BaCO_3$ (analytical grade, dried at 673 K), and CuO (extra purity grade). The materials (atomic ratio Y : Ba : Cu = 1 : 2 : 3) were milled in an agate mortar under ether, pressed into pellets, and sintered in air in a three-stage process with intermediate regrinding and repelletizing. The first sintering was at 1073 K for 72 hr, the second one at 1123 K for 24 hr, and the final at 1173 K for 48 hr. This procedure resulted in XRD single-phase samples (for X-ray powder diffraction analysis a Guinier camera with Cu$K\alpha$ radiation was used). Iodometric analysis as described by Appelman *et al.* (6) was used for calculations of the oxygen content in the $YBa_2Cu_3O_y$ samples.

2.2. Vapor Pressure

For the static vapor pressure measurements an experimental device was used with a quartz zero-point Bourdon gauge and a sickle-shaped membrane. A detailed description of the equipment has been given elsewhere (7). The samples were held in the reaction chamber in an alumina crucible. The reaction vessel was etched with a 1 : 3 mixture of HNO_3 and HCl, washed thoroughly with distilled water and dried. The reaction volume was determined to within ±0.1 ml by filling it up with a measured quantity of ethanol. This liquid was selected because of its low viscosity and surface tension. Prior to each experimental run the gauge was treated at high temperature, at first in air with a gas torch, and afterward under 10^{-5} mm Hg vacuum, in a furnace (2 to 3 hr. at 1273 K). In this way the volatile impurities were pumped out and the mechanical tension of the membrane was removed. The sensitivity of the membranes used in the experiments was not worse than 0.1 mm Hg.

The temperature was measured with two Pt–Pt/Rh thermocouples placed at the extremes of the reaction vessel, one at its bottom and the other next to the upper end of the membrane. The thermocouples were linked to a digital voltmeter (model SHCH68003, precision 0.1 mcV, input

[1] To whom the correspondence should be addressed.

0022-4596/95 $12.00

resistance $\geq$10 MΩ) via a commutator which made it possible to change the polarity of the thermo-emf during the measurements to avoid errors due to a possible drift of the zero-point of the instrument. The thermocouples were prepared and calibrated against the melting points of the standard materials according to standing requirements (8). In this way the temperature measurements were accurate to within ±0.5 K. The temperature in the furnace was controlled with a standard BPT3 instrument working from an independent Pt–Pt/Rh thermocouple. A specially designed electric circuit of the furnace made it possible to regulate the temperature profile of the furnace very precisely and to maintain the reaction vessel in isothermal conditions to within 0.1–0.5 K along the 150-mm-long reaction zone.

The vapor pressure in the reaction bulb was counterbalanced by an equal pressure of argon let into the compensation chamber of the Bourdon gauge. The compensating vapor pressure was read on a standard mercury manometer (model MBP, operational range 0.1 to 1000 mm Hg, accuracy ±0.07 mm Hg). The samples were weighed on a Sartorius R200D balance with an accuracy $\pm 5 \times 10^{-5}$ g.

The experimental apparatus as an aggregate was calibrated by measuring the saturated and unsaturated vapor pressures of cadmium metal. The experimental third-law standard enthalpy of evaporation $\Delta_f H^0$ (Cd, g, 298.15 K) = 112.4 ± 0.7 kJ/mol compares very well with the tabulated value, 112.05 ± 0.63 kJ/mol (9). The mass of cadmium calculated from the unsaturated vapor pressure measurement was in accord with the weighed mass to within ±0.00025 g.

The vapor pressure measurement procedure was as follows. In an agate mortar, the pellet was crushed into small pieces (2 to 6 mm), convenient both for weighing and loading the reaction bulb. The Bourdon gauge was pumped at $\sim 10^{-5}$ mm Hg for several hours and sealed. The furnace was heated to the starting temperature, chosen so that the initial vapor pressure of a specific sample was about 5 mm Hg, and held for 8 to 12 hr at this temperature. The measurements were made with an 8 to 10 K step. The vapor pressure was read 30 min after the equilibrium was ensured at every temperature. Special experiments with heating, cooling, and isothermal exposure of the samples showed that the equilibrium in this system was attained almost simultaneously with the furnace reaching the stationary thermal conditions (30 to 40 min, depending on the temperature).

After an experimental run the sample was slowly cooled to ambient temperature, to make sure that the heating–cooling cycle was reversible, with no vapor pressure hysteresis, no residual vapor pressure, and no mechanical deformation of the membrane. Several samples were repeatedly heated and then quenched to the room temperature; the resulting vapor pressure of oxygen was measured, pumped off, the reaction vessel was resealed, and a new experimental run was started, with a new sample composition calculated from Eq. [3] (see below).

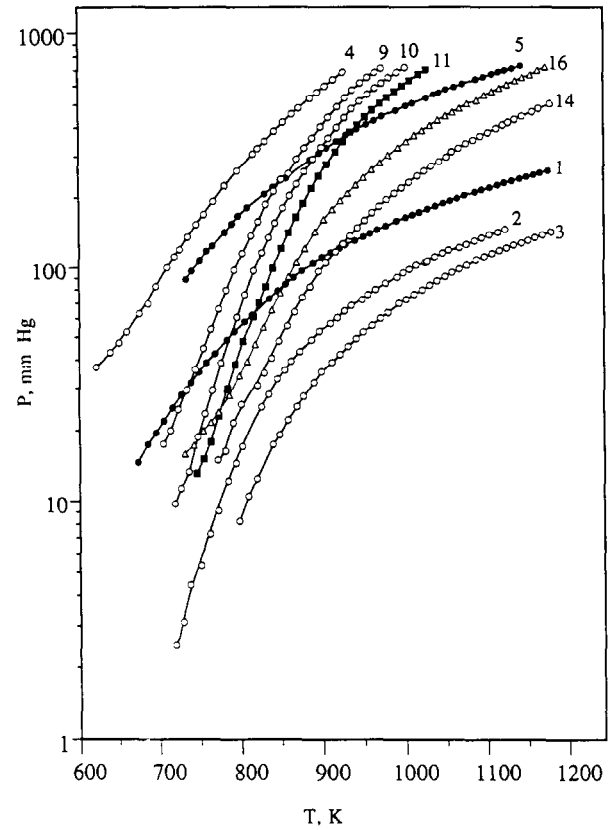

FIG. 1. Vapor pressure curves for different $YBa_2Cu_3O_y$ samples. The details are given in Table 1.

3. RESULTS

We have measured the vapor pressure as a function of the temperature for 16 samples of $YBa_2Cu_3O_y$ with different initial oxygen contents. The results are presented in Fig. 1. Numerical values of the vapor pressures (an experimental data set comprising 611 points), as well as the volume of the vapor, the initial mass of the sample, and iodometric oxygen indices, have been reported earlier (10). In the temperature range under consideration the predominant vapor species in equilibrium with $YBa_2Cu_3O_y$ is O_2. The partial pressures of other species are too small to influence the numerical results and can well be neglected in the calculations. It has also been shown (1–5, 11) that in this P–T–X range the only condensed phase is $YBa_2Cu_3O_y$, which loses oxygen on heating according to the phase reaction

$$YBa_2Cu_3O_y\ (s) \Rightarrow YBa_2Cu_3O_{y-\delta}\ (s) + 0.5\delta\ O_2(g).$$

Consequently, at a fixed cation ratio the system can be considered quasi-binary, one quasi-component being the sum of the metals and the other being oxygen. Nonstoichiometry of the crystalline phase in this system can be probed in the way described in our previous publications (see, for example, (12, 13)). It is based on an explicit argument that, when heated in a closed volume, a part of the condensed phase sublimes, and since in general the compositions of the vapor and crystal do not coincide, the solid gradually changes in composition on heating according to the expression

$$X_S = \frac{N_B - n_B}{(N_A + N_B) - (n_A + n_B)} 100\%. \quad [1]$$

Here X_S is the composition of the solid (in mol% of the component B) at the measured temperature T and vapor pressure P; N_A and N_B are the number of mols of the components (or quasi-components) A and B in the initial sample; n_A and n_B are the corresponding numbers in the vapors. By the Eq. [1] a one-to-one correspondence is established between temperature, vapor pressure, and the compositions of the conjugated condensed and vapor phases. A graphic representation of it is known as the P–T–X phase diagram of this heterogeneous equilibrium. Assuming that the vapor in equilibrium with $YBa_2Cu_3O_y$ is an ideal O_2 gas, Eq. [1] can be rewritten as

$$X_S = \frac{N_O - 2Pv/RT}{(N_M + N_O) - 2Pv/RT} 100\%, \quad [2]$$

where N_M is the total mol number of metallic elements in the sample, N_O is the initial oxygen content in the sample, v is the volume of the vapor phase, and R is the gas constant. Oxygen nonstoichiometry in oxides is usually described in terms of the oxygen index. In the vapor pressure experiment the oxygen index y at every (P, T) point is associated with the initial oxygen index y_0,

$$y = y_0 - 2Pv(a + by_0)/mRT, \quad [3]$$

where a is the total molar mass of the metals (Y + 2Ba + 3Cu), b is the atomic mass of oxygen, and m is the initial mass of the sample.

It has been shown earlier (13) that in a binary system the composition of the solid at an intersection point of two vapor pressure curves is independent of the composition of the conjugated vapor and is determined solely by the initial composition of two samples (1 and 2) and the volumes of the vapor in these two experiments:

$$X_S = \frac{N_{B1}v_2 - N_{B2}v_1}{(N_{A1} + N_{B1})v_2 - (N_{A2} + N_{B2})v_1} 100\%. \quad [4]$$

In terms of the oxygen index Eq. [4] can be rearranged:

$$y_{12} = \frac{m_1v_2y_{01}/(a + by_{01}) - m_2v_1y_{02}/(a + by_{02})}{m_1v_2/(a + by_{01}) - m_2v_1/(a + by_{02})}. \quad [5]$$

Here y_{12} is the oxygen index of the $YBa_2Cu_3O_y$ phase at the intersection point of two $P(T)$ curves for samples with initial indices y_{01} and y_{02}. Equations [4] and [5] can be used in two ways, either to determine the composition of the condensed phase at a high temperature (the intersection point) if the initial compositions are known, or to determine these initial compositions from the known X_s or y_{12}. The first approach results in a number of scanning (P, T, X_s) points on the solidus which are subsequently used to reconstruct the solidus surface in the P–T–X phase space. That is why the method is known as vapor pressure scanning of solids (12, 13).

Analysis of the experimental data showed that iodometric determination of the oxygen index is not accurate enough for quantitative interpretation of the vapor pressure results. Therefore, the experimental coordinates of the intersection points were used to determine the initial oxygen indices. They were calculated via an iteration procedure arranged so as to find the minimum of the sum of squares of residuals, $\min(\Sigma d_k^2)$, between oxygen indices calculated from Eqs. [3] and [5] at the total of n intersection points:

$$d_k^2 = (y_i - y_{ij})^2 + (y_j - y_{ij})^2 + (y_i - y_j)^2. \quad [6]$$

Here y_i and y_j were calculated from Eq. [3] and y_{ij} from Eq. [5].

Two approaches were used for this purpose. At first one of the iodometric indices, y_{01}, was used to calculate y_0 for all the other samples from Eqs. [3] and [5]; then the second, y_{02}, was used in a similar way, $y_{03}, \ldots, y_{0n}$. This first iteration cycle lead to the mean values of all y_0 which were used for a second cycle, and so on, until two conditions were met: (a) the minimum value of Σd_k^2 was reached, and (b) the difference in y_i, calculated from Eq. [3] and Eq. [5], was on the order of magnitude 10^{-3}. The second approach was to solve an overdetermined set of equations [3], [5], and $y_{0i} = y(\text{iod})$ where $y(\text{iod})$ is a set of all the iodometric indices. These two approaches lead to similar results quoted in Table 1 as y_I and y_{II}. In subsequent treatment y_I values were used, since for those the sum of squares of residuals was somewhat lower.

To find the (P, T) coordinates of the intersection points, polynomial fits $P = \Sigma a_iT^i$ of the vapor pressure curves were used for tetragonal and orthorhombic phases separately. The phase transition showed on the vapor pressure curve as a breaking point in the $\log P = f(1/T)$ representation (dashed line in Fig. 2).

TABLE 1
Iodometric Results (y_{iod})[a] and Vapor Pressure Determination of Oxygen Indices in the $YBa_2Cu_3O_y$ Samples

Exp.	m (g)	v (ml)	y_{iod}	y_I	δy_I	y_{II}
1	0.93666	135.7	6.97	6.934	0.003	6.932
2	0.93060	135.7	6.70	6.673	0.006	6.667
3	0.92847	135.6	6.60	6.589	0.007	6.573
4	1.96508	33.6	6.97	6.934	0.003	6.932
5	0.84895	36.9	6.97	6.977	0.004	6.978
6	0.85643	48.0	6.74	6.698	0.005	6.697
7	0.85561	48.0	6.69	6.665	0.005	6.659
8	0.85268	48.0	6.56	6.526	0.005	6.523
9	3.18785	47.3	6.78	6.809	0.004	6.809
10	3.18472	47.3	6.74	6.765	0.004	6.764
11	3.18126	47.3	6.70	6.720	0.004	6.721
12	1.38649	34.7	—	6.819	0.004	6.819
13	1.38363	34.7	—	6.730	0.004	6.731
14	0.95111	35.4	6.60	6.633	0.006	6.631
15	1.19842	30.7	6.86	6.866	0.004	6.868
16	1.19249	30.6	6.65	6.683	0.006	6.670
Sum of squares of residuals at the intersection points			0.20	3.25×10^{-3}		4.01×10^{-3}

Note. Two calculation procedures (y_I and y_{II}) are described in the text.
[a] Iodometric analysis was made by G. N. Mazo (Moscow State University).

An independent check of the initial composition of the samples can be made if the composition of the condensed phase at the intersection point is written in wt.% of the nonvolatile component M,

$$X_s(\text{wt.\% } M) = \{G_M/(G - g)\} \times 100\%, \quad [7]$$

where G_M is the mass of the nonvolatile component in the sample, G is the total mass of the sample, and g is the mass of the vapor phase, which in the case of pure oxygen is equal to $g = 32Pv/RT$. Thus, at the intersection point (P, T) of two vapor pressure curves (1 and 2) where, according to Eq. [4], the composition of the condensed phase should be the same for both curves, the mass ratio of the nonvolatile component in the two samples is

$$\frac{G_{M1}}{G_{M2}} = \frac{G_1 - g_1}{G_2 - g_2}. \quad [8]$$

In the case under consideration G_{Mi} is the total mass of the metallic elements in the sample i irrespective of the actual ratio between Y, Ba, and Cu in it. On the other hand, G_{Mi} can be calculated for each sample i from the total mass of the sample G_i and the oxygen index y_{0i} as

$$G_{Mi} = \frac{aG_i}{a + by_{0i}} \quad [9]$$

Comparison of the results from Eq. [8] and Eq. [9] is a measure of confidence in the oxygen indices calculated from Eq. [5] and the initial assumption of the quasi-binary behavior of the system. The actual calculations showed that the G_{Mi}/G_{Mj} ratios were well within the limits of experimental weighing errors of the balance used for preparation of the material.

4. DISCUSSION

Once all the initial oxygen indices were found, each experimental run provided a set of (P, T, X_s) points, and

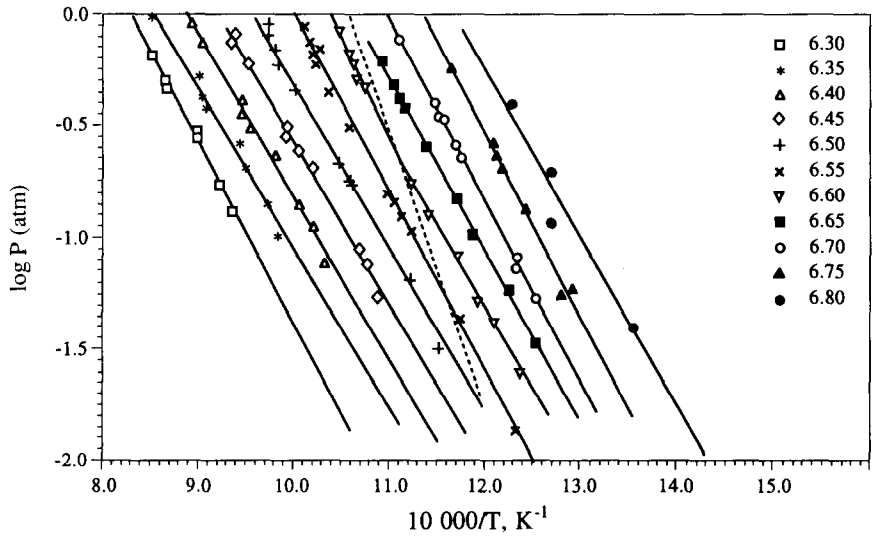

FIG. 2. Temperature dependencies of the oxygen pressure for different oxygen indices in $YBa_2Cu_3O_y$. The dashed line represents the experimental tetragonal ⇔ orthorhombic phase transition.

TABLE 2
Polynomial Fits $x = \sum a_i(10^3/T)^i$ for $YBa_2Cu_3O_{7-x}$ at Different Oxygen Pressures

P (atm)	a_0	a_1	a_2	a_3	T (K)
0.01	5.81881	−6.79265	2.01781	—	625–813
0.10	−5.97506	20.0794	−19.0581	5.58962	685–1050
0.21	−2.78437	12.4477	−13.2767	—	735–1250
0.50	1.93452	−1.43321	8.6021×10^{-3}	—	820–1190
1.00	1.75304	−1.20839	−0.10144	—	940–1190

all the experimental data resulted in 611 scanning points from which the solidus surface of the $YBa_2Cu_3O_y$ phase was reconstructed in the P–T–X phase space.

The space arrangement of the solidus was determined in an analytical form. For this purpose sections of the space model were made by three orthogonal planes, T = const, P = const, and X_s = const. To do this, the following polynomial fits of each vapor pressure curve i were made: $P_i(T)$, $T_i(P)$, $X_{si}(T)$, $T_i(X_s)$, $P_i(X_s)$, and $X_{si}(P)$. Isobaric sections were derived from a set of equations $\{X_{si} = X_{si}(P), T_i = T_i(P)\}$ solved for several pressures and presented in Table 2. In a similar way, sets of equations $\{X_{si} = X_{si}(T), P_i = P_i(T)\}$ and $\{T_i = T_i(X_s), P_i = P_i(X_s)\}$ were solved for a number of temperatures and compositions of the solid to obtain isothermal and isoplethal (X_s = const) sections. The corresponding results are listed in Tables 3 and 4. The isopleths are shown separately in Fig. 2.

In Table 5 partial molar functions of oxygen, calculated from the vapor pressure data, are compared with the corresponding values derived from different thermogravimetric experiments. It can be seen in Table 5 that, although different TGA measurements do not coincide with each other, they tend to lead to higher thermodynamic functions as compared to the values derived from the vapor pressure data. Two main reasons could be responsible for this discrepancy: uncertainties in the initial oxygen index and nonequilibrium conditions of the TGA measurements. The latter is expected to be the more probable the lower are the temperature and the pressure (1). This should lead to progressive underestimation of the vapor pressure with decreasing temperature and, as a consequence, to higher slopes of the $P(T)$ functions resulting in overestimated enthalpy values. This is exactly what is seen in Table 5; our equilibrium results produced lower H_{O_2} values than those calculated from TGA. One more factor could lead to this discrepancy; the majority of the log $P(1/T)$ TGA straight lines in (1–5), from which the H_{O_2} and S_{O_2} values were derived, were drawn through three to four (P, T) points, some of them even through two points, whereas our data originated in 7 to 13 (P, T) points, which is a statistically representative set of data. A tendency can be seen in Table 5 for H_{O_2} to increase when the oxygen index approaches $y = 6$. This trend was also noted by Yamaguchi *et al.* (3), both for $y = 6$ and $y = 7$ extremes.

TABLE 3
Isopleths of the Oxygen Pressure, $\log(P_{O_2}\ (\text{atm})) = A - B/T$, for $YBa_2Cu_3O_y$

y	A	B	T (K)
	Tetragonal phase		
6.30	6.58 ± 0.62	7900 ± 700	940–1205
6.35	6.01 ± 0.79	7100 ± 900	900–1175
6.40	6.33 ± 0.45	7100 ± 500	870–1130
6.45	6.59 ± 0.45	7200 ± 400	850–1075
6.50	6.91 ± 0.43	7200 ± 400	830–1040
	Orthorhombic phase		
6.65	8.14 ± 0.36	7700 ± 300	770–925
6.70	8.82 ± 0.52	8000 ± 400	760–910
6.75	9.30 ± 1.15	8200 ± 900	730–875
6.80	9.29 ± 0.59	7900 ± 500	700–845
6.85	9.89 ± 1.72	8000 ± 1300	680–805

TABLE 4
Isotherms of the Oxygen Pressure for the $YBa_2Cu_3O_{7-x}$ Phase

	Orthorhombic phase, $P(\text{atm}) = \sum a_i x^i$					
T (K)	a_0	a_1	a_2	a_3	a_4	x
773	4.23600	−54.4900	267.892	−588.223	483.561	0.10–0.39
823	6.90307	−68.2045	257.467	−434.449	274.587	0.16–0.40
873	8.61699	−61.3831	159.423	−168.689	52.7924	0.24–0.44
	Tetragonal phase, $P(\text{atm}) = \alpha \times x^\beta$					
T (K)		$\alpha \times 10^2$		β		x
873		0.10364		−5.35623		0.44–0.55
923		0.24087		−5.61639		0.38–0.62
973		0.37233		−6.40011		0.41–0.68
1023		0.67373		−6.83363		0.49–0.73
1073		1.29981		−6.97083		0.53–0.76
1123		1.94813		−7.59700		0.59–0.80
1173		2.50969		−8.84175		0.66–0.80

The discrepancy between different P–T–X results is clearly seen in Fig. 3, where our data, shown as fits for a number of oxygen pressures, is compared with some of the TGA publications. At higher temperatures and pressures our data coincides with TGA within the limits of different TGA results ($\Delta y = \pm 0.02$ and $\Delta T = \pm 10$ K (1)), whereas at $P = 0.01$ atm this disagreement increases up to ±0.08 and ±40 K.

5. CONCLUSION

An extensive vapor pressure study of the oxygen nonstoichiometry in $YBa_2Cu_3O_y$ as a function of temperature and oxygen pressure is reported. Special attention was

TABLE 5
Partial Molar Oxygen Enthalpies H (kJ/mol) and Entropies S (J/mol × K) for $YBa_2Cu_3O_y$

	Our data		(1)		(2)		(3)	(4)		(5)	
y	$-S_{O_2}$	$-H_{O_2}$	$-S_{O_2}$	$-H_{O_2}$	$-S_{O_2}$	$-H_{O_2}$	$-H_{O_2}$	$-S_{O_2}$	$-H_{O_2}$	$-S_{O_2}$	$-H_{O_2}$
					Tetragonal phase						
6.30	126	152	122	155	144	173	169	121	153	117	148
6.40	121	137	140	162	148	166	160	132	157	128	148
6.50	132	138	160	170	171	176	164	131	144	136	146
					Orthorhombic phase						
6.60	154	149	170	169	196	188	166	157	159	159	157
6.70	169	154	179	165	211	190	172	171	162	169	157
6.80	178	151	188	162	220	184	173	—	—	187	162

given to ensure the equilibrium conditions of the measurements. Iodometric analysis was shown to be essentially less accurate than the vapor pressure method and therefore was used only as a first approximation for determination of oxygen in $YBa_2Cu_3O_y$. With the reported data taken as a standard, vapor pressure scanning can be used as a powerful analytical method for the precise determination of oxygen in the $YBa_2Cu_3O_y$ phase.

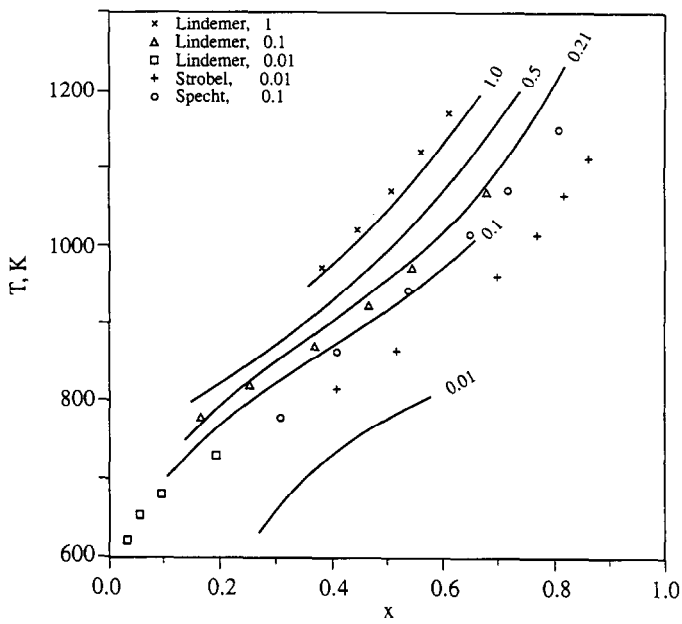

FIG. 3. Isobars of the oxygen pressure for the $YBa_2Cu_3O_y$ phase. The numbers correspond to the vapor pressures (atm). The smooth curves are fits of our experimental data. The points represent TGA measurements reported by Lindemer *et al.* (1), Strobel *et al.* (4), and Specht *et al.* (5).

ACKNOWLEDGMENT

J. H. Greenberg would like to thank Professor L. Ben-Dor for cooperation and support.

REFERENCES

1. T. B. Lindemer, J. F. Hunley, J. E. Gates, A. L. Sutton, J. Brynestad, C. R. Hubbard, and P. K. Gallagher, *J. Am. Ceram. Soc.* **72,** 1775 (1989).
2. K. Kishio, K. Suzuki, T. Hasegawa, T. Yamamoto, and K. Kitazava, *J. Solid State Chem.* **82,** 192 (1989).
3. S. Yamaguchi, K. Terabe, A. Saito, S. Yahagi, and Y. Iguchi, *Jpn. J. Appl. Phys.* **27,** L179 (1988).
4. P. Strobel, J. J. Capponi, and M. Marezio, *Solid State Commun.* **64,** 513 (1987).
5. E. D. Specht, C. J. Sparks, A. G. Dhere, J. Brynestad, O. B. Cavin, D. M. Kroeger, and M. A. Oye, *Phys. Rev. B Condens. Matter* **37,** 7426 (1988).
6. E. H. Appelman and L. R. Morss, *Inorg. Chem.* **26,** 3237 (1987).
7. V. B. Lazarev, J. H. Greenberg, and B. A. Popovkin, *in* "Current Topics in Materials Science" (E. Kaldis, Ed.), Vol. 1, pp. 657–695. Elsevier, Amsterdam/New York (1978).
8. D. Kamke and K. Kremer, "Physical Basis of Numerical Measurements." Mir, Moscow, 1980.
9. R. Hultgren, R. L. Orr, P. D. Anderson, and K. K. Kelley, "Selected Values of Thermodynamic Properties of Metals and Alloys." New York/London, 1963.
10. I. V. Tarasov, V. N. Guskov, V. B. Lazarev, O. V. Shebershneva, and M. L. Kovba, "Vapor Pressure of $YBa_2Cu_3O_y$: Experimental Data." VINITI, Moscow, 1993.
11. V. B. Lazarev, K. S. Gavrichev, V. E. Gorbunov, and J. H. Greenberg, *Thermochim. Acta* **174,** 27 (1991).
12. J. H. Greenberg, V. B. Lazarev, and V. N. Guskov, *Proc. Acad. Sci. USSR* **262,** (2), 371 (1982).
13. J. H. Greenberg and V. B. Lazarev, *in* "Current Topics in Materials Science" (E. Kaldis, Ed.), Vol. 12, pp. 119–204. Elsevier, Amsterdam/New York (1985).